Article

Characterizations and Use of Recycled Optical Components for Polarizing Phase-Shifting Interferometry Applications [†]

Juan M. Islas-Islas [1], Germán Reséndiz-López [1,2], José G. Ortega-Mendoza [2], Luis García-Lechuga [1], Adolfo Quiroz [3], David-Ignacio Serrano-García [4], Benito Canales-Pacheco [5] and Noel-Ivan Toto-Arellano [1,*]

[1] Cuerpo Académico de Ingeniería Ciencias e Innovación Tecnológica, Universidad Tecnológica de Tulancingo, Hidalgo 43645, Mexico; manuel.islas@utectulancingo.edu.mx (J.M.I.-I.);
gresendizl@utectulancingo.edu.mx (G.R.-L.); luis.garcia@utectulancingo.edu.mx (L.G.-L.)
[2] Universidad Politécnica de Tulancingo, Hidalgo 43629, Mexico; jose.ortega@upt.edu.mx
[3] Universidad Tecnológica de la Xicotepec de Juarez, Puebla 73080, Mexico; adolfo.quiroz@utxicotepec.edu.mx
[4] University Center for Exact Sciences and Engineering (CUCE), Guadalajara University, Hidalgo 44430, Mexico; david.serrano@academicos.udg.mx
[5] Universidad Tecnológica de la Sierra Hidalguense, Hidalgo 43200, Mexico; benito.canales@utsh.edu.mx
* Correspondence: noel.toto@utectulancingo.edu.mx
[†] This paper is dedicated to the memory of our marvelous colleague, Doctor Gustavo Rodríguez Zurita. "That person who helps others simply because it should or must be done and because it is the right thing to do, is genuine without a doubt, a real superhero (SL)".

Abstract: In this research, we report using optical components such as cubic beam splitters, lenses, diffraction gratings, and mirrors from broken, obsolete, or disused electronic devices to implement a simultaneous polarization-based phase-shifting interferometric system. The system is composed of a polarized Mach–Zehnder interferometer (PMZI) which generates a sample pattern coupled to a 4f imaging system with a diffraction grating placed on its Fourier plane. Such a diffractive element replicates the pattern generated by the PMZI, and each replica is centered and modulated by each diffraction order generated by the grating. The corresponding individual phase shifts are controlled by placing linear polarizers with known angles in front of each replica. Experimental results are presented using several phase samples such as an oil drop, a pseudoscorpion claw, a microarthropod, and red blood cells. In addition, a comparison of the retrieved phase was conducted by employing two different phase demodulation algorithms.

Keywords: interferometry; phase shifting; polarization

1. Introduction

In the last few decades, the so-called brown economic model caused the depletion of natural resources, degradation, and widespread loss of ecosystems. As a response, an alternative economic model emerged called the green economy. An essential part of the green economy model is the circular economy practice of reducing, reusing, and recycling (3R scheme) [1,2]. Following this 3R scheme, we implemented a polarization-based phase-shifting interferometric system using recovered optics from electronic waste [3].

Today, throwing away CD/DVD reading devices and broken or obsolete projectors is prevalent. However, those devices are sources of good-quality optical components such as lenses, mirrors, diffraction gratings, cubic beam splitters, polarizer sheets, and Fresnel lenses, among others that can be used in the implementation of interferometric systems. Currently, several industrial sectors and academic fields incorporate optical and photonic technologies for quality inspection metrics [4–7]; therefore, it is important to develop interferometric techniques and devices capable of contactless high-precision measurements applied to phase objects [4–10].

There are a wide variety of techniques to perform these measurements, mainly based on the recovery of the optical phase. Several methods are applied in this field, with Fourier

and phase-shifting techniques among the most common. Phase-shifting interferometry is not new; however, several used techniques conventionally generate phase shifts in stages by using piezoelectric transducers, diffractive elements, or actuators, having the limitation of being applied only for static samples.

Several authors and companies have developed techniques of simultaneous phase-shifting based on the use of diffractive elements, micro-polarizer arrays, or systems with four synchronized cameras for simultaneously detecting four controllable phase-shifted interferograms. However, each system presents advantages and disadvantages. Some systems are not easily acquired, such as a micro-polarizer array aligned with a CCD sensor or a synchronization unit for several cameras capturing each interferogram separately [11–13].

Considering the above, we implemented a PMZI coupled to an imaging system that uses a diffraction grating. Previous reports have implemented several interferometric systems, such as a double-window interferometer coupled to a 4f imaging system [13,14]. In these cases, the interferograms are generated by superimposing diffraction orders of the replicas having the disadvantage of common polarization errors on the beams of the double window caused by the separation of the windows.

The system proposed here has the advantage of generating a base interferogram with known polarization properties; hence, the 4f system works as a pattern replicator [13,14]. Manufactured bases and supports were used in a previous report, and another arrangement was presented to generate the interferogram (Michelson interferometer) [13]. In this work, a Mach–Zehnder interferometer configuration was used, because it facilitates the placement of the samples with such small components. We also used bases and supports designed in CAD and produced by considering the recycled components.

The development of these implemented low-cost interferometric systems can serve as a valuable tool for several applications, such as determining the transmittance distributions of cells or their morphology to diagnose diseases. Moreover, it could be helpful to analyze microscopic transparent samples, such as cells, tissue, wavefronts [15–20], and thin films, in a noninvasive way, as well as the visualization of thin-film surfaces or phase changes of a refractive index in-phase samples [21–23]. The recovered optics has the minor disadvantage of being small (mm scales), since the most significant component (cubic beam splitter) is no larger than 5 mm. Most miniature lenses are ~3 mm in diameter, limiting the implemented systems to measuring samples of such scales. Nevertheless, these low-cost interferometers are perfect for physics and optics microscopic samples and educational purposes.

2. Recovery of Optical Components from Electronic Waste

In order to use recycled components, we had to measure and characterize their properties using known optical techniques [23–26]. The cubic beam splitters had a scale of 5 mm × 5 mm, obtained from the DVD readers. For their characterization, we measured the power of the reflected and the transmitted light, obtaining 40% transmittance and 60% reflectance. We also checked the degree of polarization by collocating a polarizer as an analyzer and measuring the optical power with a potentiometer; since there was no variation in the intensities, we concluded that the beam splitter was nonpolarized. The recovered diffraction gratings had a scale of 3 mm × 3 mm, and their characterization consisted of measuring their period $d \approx 6.62$ µm. To implement the 2D gratings, we placed two gratings with their transmission axes orthogonally fixed.

One of the main disadvantages when handling such small optical components (ranging between 2 and 5 mm) is a longer alignment time. For this reason, an acrylic plate (also recovered from the garbage) was used to implement custom supports and bases for the components. The modeling of these parts was carried out in design software (SolidWorks), and the pieces were later cut using a laser cutting machine (LX-6090 elite). We also carried out the assembly of the pieces. In Figure 1, the bases and supports implemented for the recycled optical components are shown. Table 1 shows the optical components and electronic waste from which they were recovered (from a DVD reader), with their measured properties.
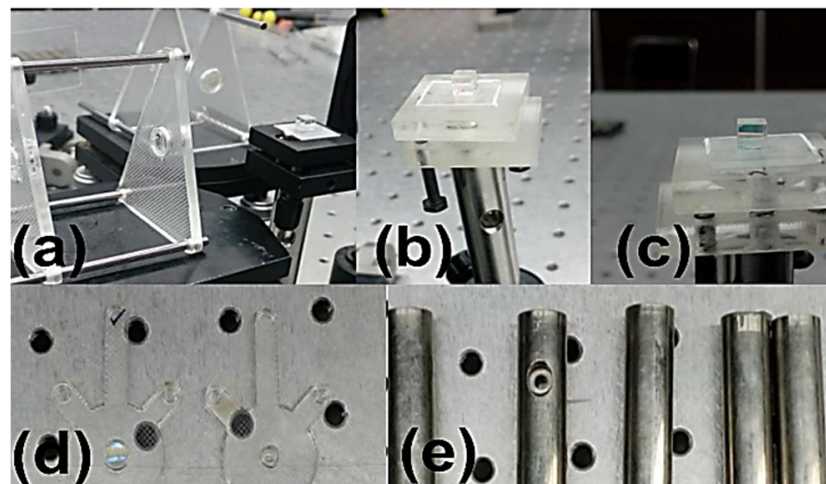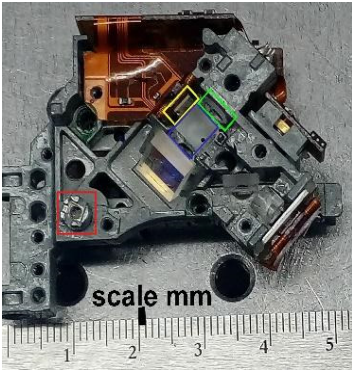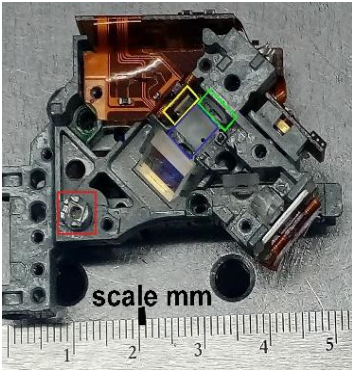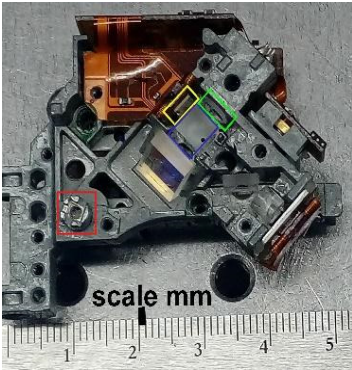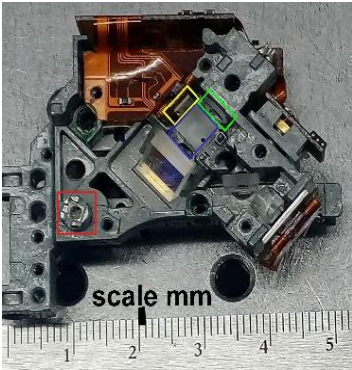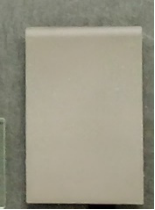
Figure 1. Bases, posts, and supports for optical components. (**a**) Lens holders. (**b**,**c**) Bases with *xy* movement for a cube beam splitter. (**d**) Laser-cut components parts. (**e**) Posts cut with CNC lathe.

Table 1. Characteristics of optical components recovered from recycled electronics.

DVD Reader	Optical Component	Characteristics		Scale
		Polarizing	Non	
	Beam splitter	Reflectivity	60%	5 mm × 5 mm
		Transmittance	40%	
	Lens	Focal	5 mm	3 mm diameter
		Thickness	3 mm	
	Diffraction grating	Period 6.62 μm		3 mm × 3 mm
	Mirror	Thickness	3.0 mm	10 mm × 20 mm
		Reflectance (normal incidence)	92%	

3. Grating Interferometry

The proposed system is shown in Figure 2; it consists of a polarized Mach–Zehnder interferometer (PMZI, see Figure 2a) that generates the overlap of beams A (phase object) and B (reference), both with opposed circular polarizations, which can be expressed as

$$\vec{A} = \vec{J}_L e^{i\varphi(x_0,y_0)} \quad \vec{B} = \vec{J}_R, \tag{1}$$

where $\vec{J}_L$ has a left circular polarization and $\vec{J}_R$ has right circular polarization, defined as follows:

$$\vec{J}_L = \frac{1}{\sqrt{2}} \begin{pmatrix} 1 \\ i \end{pmatrix} \text{ and } \vec{J}_R = \frac{1}{\sqrt{2}} \begin{pmatrix} 1 \\ -i \end{pmatrix}, \tag{2}$$

where $\varphi(x_0, y_0)$ is the optical phase introduced by the phase object, in the object plane. When the beams of Equation (1) overlap and pass through a linear polarizer $P(\psi)$, placed at an angle ψ [27,28], we obtain the intensity of the base pattern as

$$I(x_0, y_0) = \left| P(\psi) \cdot \vec{A} + P(\psi) \cdot \vec{B} \right|^2, \tag{3}$$

where $P(\psi)$ is the linear polarizing transmission matrix given by

$$P(\psi) = \begin{pmatrix} \cos^2 \psi & \sin \psi \cos \psi \\ \sin \psi \cos \psi & \sin^2 \psi \end{pmatrix}. \tag{4}$$

The resulting irradiance can be written as

$$I_0(x, y) = I_1 + I_2 + 2\sqrt{I_1 I_2} \cos[2\psi - \Delta\varphi(x_0, y_0)], \tag{5}$$

where $\Delta\varphi(x_0, y_0)$ is the phase difference, while the phase shift can be controlled by operating the polarizer angle according to the following relation:$\xi = 2\psi$.
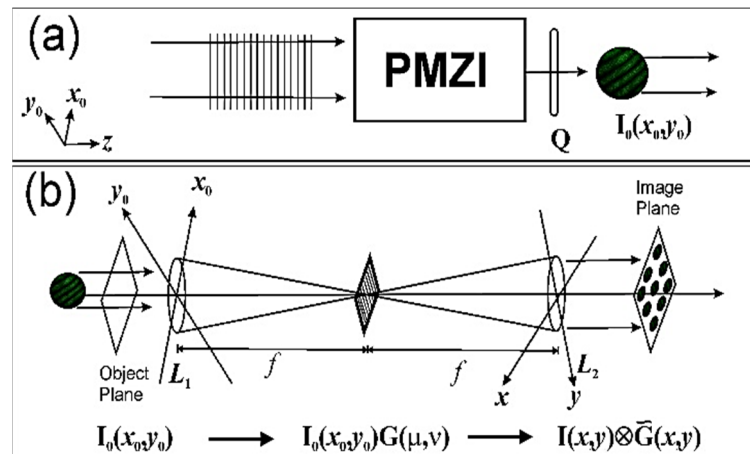
Figure 2. System diagram. (**a**) Pattern generated by the PMZI. (**b**) Replication of the patterns by the 4f diffraction grating system.

3.1. Pattern Replication with 2D Gratings

The amplitude gratings placed on the Fourier plane can be mathematically formulated in 2D as follows:

$$\begin{aligned} G(\mu, v) = &\sum_{n=-N}^{N} \text{Rec}t\left[\frac{\mu}{w}\right] \otimes \delta\left(\frac{\mu - nd}{w}\right) \times \\ &\sum_{l=-L}^{L} \text{Rec}t\left[\frac{v}{w}\right] \otimes \delta\left(\frac{v - ld}{w}\right) \end{aligned}, \tag{6}$$

where w is the width of the clear strips, N, L are the numbers of components of the grating, and d is the respective spatial period along directions μ and v. Thus, the Fourier transform of Equation (6) with $N, L \rightarrow \infty$ is given by

$$
\begin{aligned}
\widetilde{G}(x,y) \;=\; & \frac{w^2}{d^2} \sin c(wx) \sum_{n=-N}^{N} \delta\left(x - \frac{n}{d}\right) \\
& \times \sin c(wy) \sum_{L=-l}^{l} \delta\left(y - \frac{l}{d}\right)
\end{aligned}
\tag{7}
$$

where $x = -x_0/\lambda f$ and $y = -y_0/\lambda f$ are the coordinates in the image plane.

3.2. Coupled 4f Imaging System

The output of the PMZI generates the pattern with two beams with orthogonal circular polarization states to be replicated. As can be seen in Figure 2b, a $4f$ system with 2D grating is used to multiplex the pattern. In this case, the interference pattern defined by $I_0(x_0,y_0)$ impinges onto the first transformer lens (L_1); hence, in the Fourier plane of the $4f$ system, we obtain the product of $I_0(x_0,y_0)$ and $G(\mu,v)$ functions. Then, the second transformer lens (L_2) receives the Fourier transform; hence, in the image plane, we obtain the convolution of the interference pattern with the Fourier transform of the grating. The interference pattern $I(x,y)$ on the image plane of the system becomes

$$
I(x,y) = I_0(x_0,y_0) \otimes \left|\widetilde{G}(x,y)\right|^2.
\tag{8}
$$

Physically, in the image plane, we observe centered interference pattern replicas around each diffraction order generated by the grating, represented as

$$
I(x,y) = \{\sin c(wx)\sin c(wy)\} \times \left\{ I_1 + I_2 + 2\sqrt{I_1 I_2}\cos[2\psi - \varphi(x,y)]\right\}.
\tag{9}
$$

Equation (9) shows that the resulting replicas of the pattern generated by the system are displaced and modulated by the diffraction orders generated by the grating [13,14,27]. The interference pattern's phase shifts (ζ) can be generated by operating the linear polarizers placed at an angle ψ. The intensity of the beam pattern can be obtained as

$$
I(x,y) = A^2 + B^2 + 2AB\cos[2\psi - \varphi(x,y)],
\tag{10}
$$

where A^2 and B^2 correspond to the irradiances of the object and the reference beam respectively, both modulated by the grating diffraction orders, defined as

$$
A^2 = I_1 \sin c(wx)\sin c(wy), \;\; B^2 = I_2 \sin c(wx)\sin c(wy).
\tag{11}
$$

3.3. Optical Phase Recovery Algorithm

In this work, we used the well-known four-step algorithm operated with interferograms, obtained by placing linear polarizers at the angles $\psi_1 = 0°$, $\psi_2 = 45°$, $\psi_3 = 90°$, and $\psi_4 = 135°$, in front of each replica to generate the respective phase shifts of $0°$, $90°$, $180°$, and $270°$ [9,14,28]. Thus, we can generate four simultaneous interference patterns spatially separated in the same image given by

$$
\begin{aligned}
I_1(x,y) &= A^2 + B^2 + 2AB\cos[\varphi(x,y)] \\
I_2(x,y) &= A^2 + B^2 + 2AB\sin[\varphi(x,y)] \\
I_3(x,y) &= A^2 + B^2 - 2AB\cos[\varphi(x,y)] \\
I_4(x,y) &= A^2 + B^2 - 2AB\sin[\varphi(x,y)]
\end{aligned}
\tag{12}
$$

and the optical phase is obtained as follows [29,30]:

$$\tan \varphi(x,y) = \left[\frac{I_2 - I_4}{I_1 - I_3} \right]. \tag{13}$$

For this case, the evaluated phase is wrapped between $[-\pi, \pi]$ due to the arctangent function, and, to remove the background phase [31,32], we should measure a reference phase map beforehand. We employed the Quality-Guided Path Following Method for unwrapping the phase [32]. To show that more interferograms can be used and to make a comparison, we used two interferograms to calculate the relative phase using the Vargas–Quiroga method [33], which requires a constant phase shift between the interferograms that can vary between the values of 0 to 2π. For this case, each step ξ was taken every $60°$; thus, values of ψ_n were $\psi_1 = 0°$, $\psi_2 = 30°$.

4. Experimental Setup

The implemented experimental system based on a polarized Mach–Zehnder interferometer (PMZI) coupled to a *4f* system with a diffraction grating in the Fourier plane is shown in Figure 3. A laser beam emerging from a laser source (λ = 530 nm) with orthogonal linear polarization is filtered by the spatial filtering system (SFS), to later be collimated by the L_0 lens (f = 3 mm), which generates a plane wavefront that impinges on the PMZI. In the MZI, the transmitted beam is arm A, where the phase object (PO) is placed, and then a linear polarizer (P_1) at $90°$ with respect to the x_0-axis generates orthogonal polarization. The reflected beam is arm B, which is polarized parallel to the x_0-axis ($0°$) with the linear polarizer P_2.
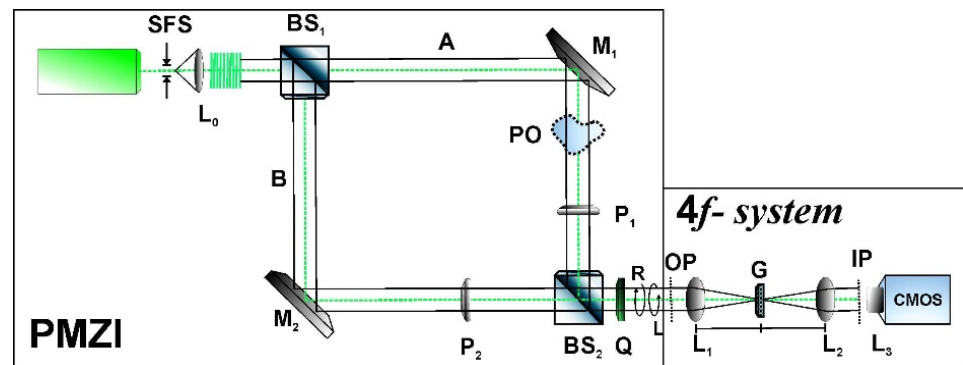

Figure 3. Experimental setup. Laser operating at 532 nm. SFS: spatial filter system. L_0: collimated lens. Pi: linear polarizers. M_i: mirrors. BS: beam splitter. Q: quarter-wave plate. G: 2D grating. L_1, L_2: lenses of *4f* system. L_3: zoom lens. IP: image plane. PO: phase object.

The two beams recombine in BS_2 and emerge from the MZI with polarizations orthogonal to each other; at the output of the MZI, they impinge on a quarter-wave plate (Q) with its fast axis at $45°$ with respect to the x_0-axis. This generates circular polarizations to the left (L) and to the right (R). At the exit of the PMZI, we coupled a *4f* system with a 2D diffraction recycled grating (G) at the Fourier plane in order to generate the replicas of the incident pattern. This result is obtained because of the modulation generated by Fourier coefficients, due to the replicas of the interference patterns centered around each diffraction order according to Equation (9). The replicas are observed in the image plane (IP), where the polarizer mask is placed with four linear polarizers at angles of $0°$, $45°$, $90°$, and $135°$ in a rectangular arrangement in a clockwise direction.

5. Results

The imaging system consists of a 3.0 MP CMOS sensor with 2048×1536 pixels (pixel size, 3.2 μm $\times$ 3.2 μm); the CMOS camera is adjusted to simultaneously capture the images of four interference patterns. In order to use the recycled components, there was a selection

process based on their characterization (shown in Table 1). It is worth mentioning that it was a "handicraft" work, since many of the recovered components were not useful or suffered damage at the moment of detaching them from their base or support, such as scratches or glue spots that made them useless; in particular, most of the gratings showed scratches that generated very noisy images in the diffraction pattern. Therefore, out of ~100 components, we searched for those that did not introduce noticeable noise distortions. Because of this, we mention in the manuscript that these components can only be used for basic research or education since it is somewhat tedious to search for recycled components.

The interferogram was recorded with a resolution of 400 × 400 pixels. To generate the independent phase shifts, we used a polarizer mask with four polarizers in the arrangement, which were made by cutting a polarizing sheet. The cut of the polarizers was done with a laser cutting machine; for the placement of the polarizers at the appropriate angles, a calibrated polarizer was used as an analyzer, and the transmitted intensities were measured. We checked circular polarizations in every pattern by verifying that the intensity did not vary with the analyzer rotation, guaranteeing that the correct phase shifts would be obtained [14,34–40]. As we used diffractive elements to generate the simultaneous interferograms, some patterns showed minimal variations in intensities. For this reason, it was necessary to use a pre-filtering process in order to eliminate the background, normalize the amplitude modulation, and filter out noise [41,42]. Figures 4–6 show the results obtained with phase samples such as wavefronts and synthetic components. Figures 7–9 show the results obtained with microscale biological samples.
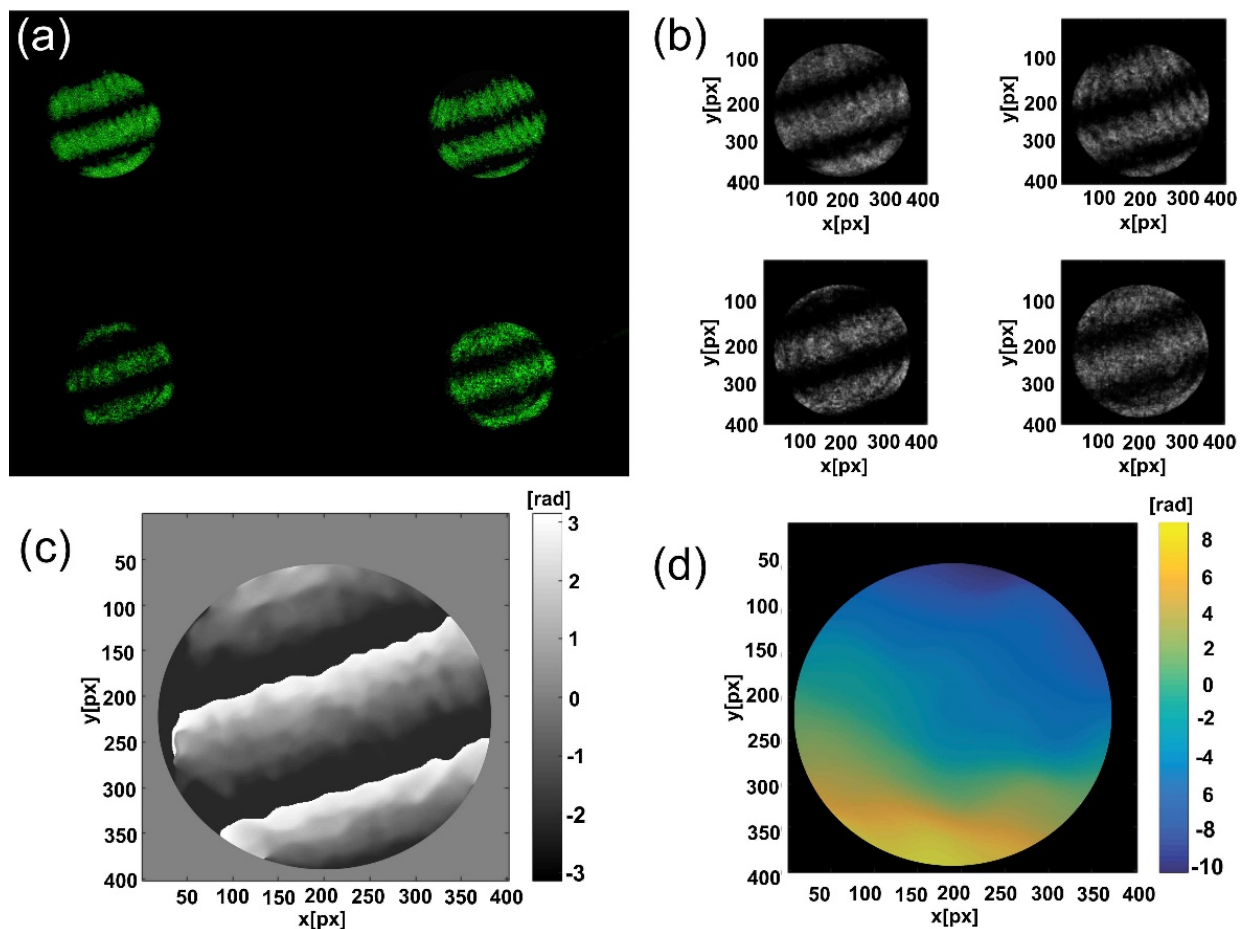

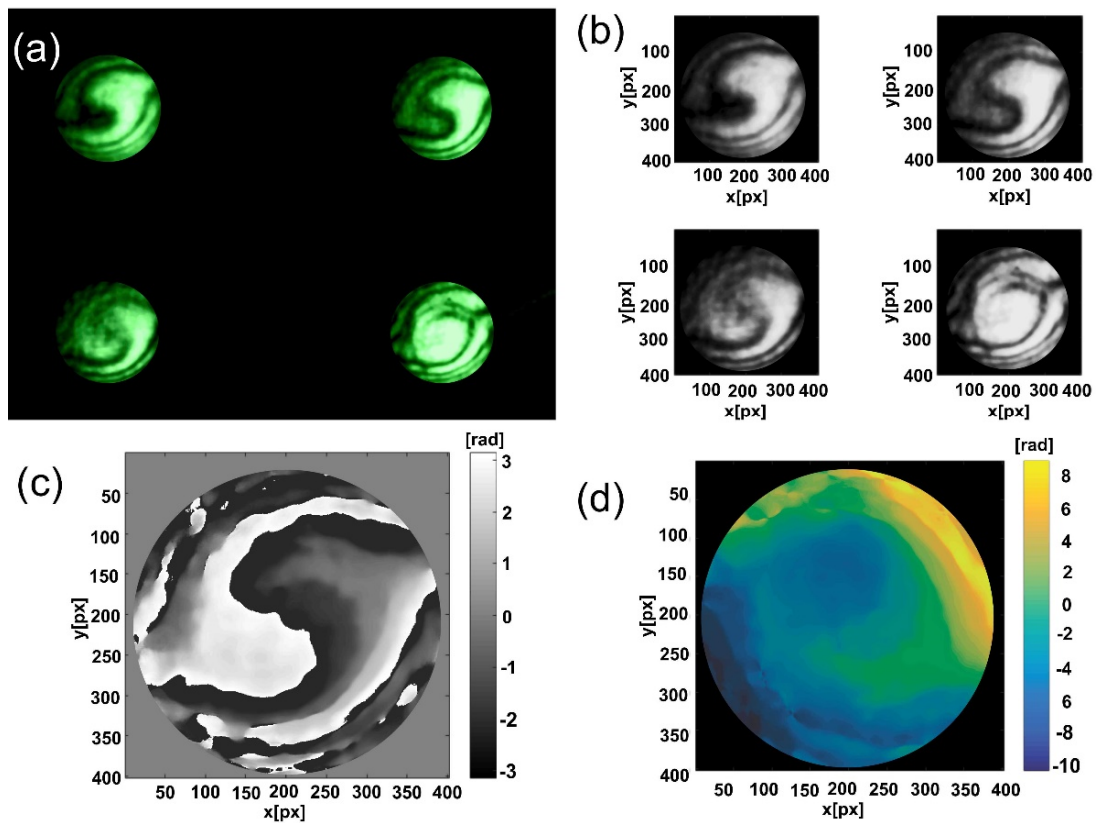**Figure 4.** Tilted wavefront. (**a,b**) Four simultaneous patterns. (**c**) Wrapped phase. (**d**) Phase map.

Figure 5. Lens out of focus and off the optical axis. (**a**,**b**) Four simultaneous patterns. (**c**) Wrapped phase. (**d**) Phase map.
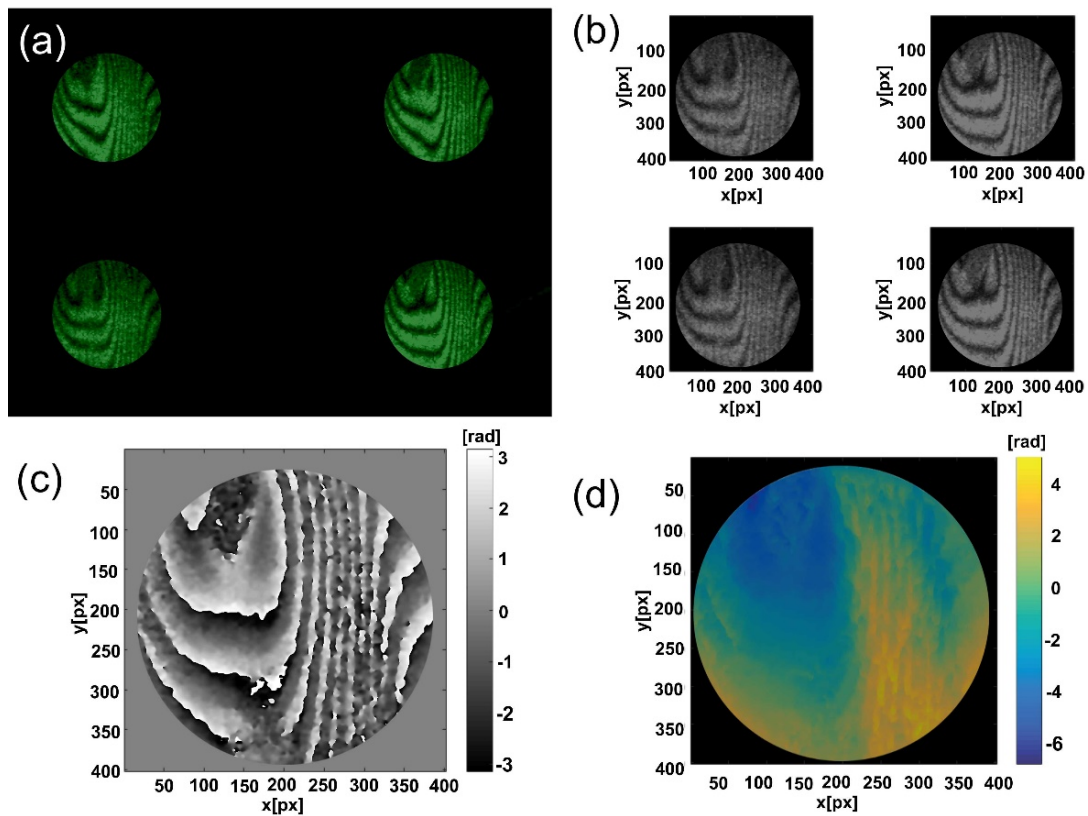
Figure 6. Oil layer. (**a**,**b**) Four simultaneous patterns. (**c**) Wrapped phase. (**d**) Phase map.
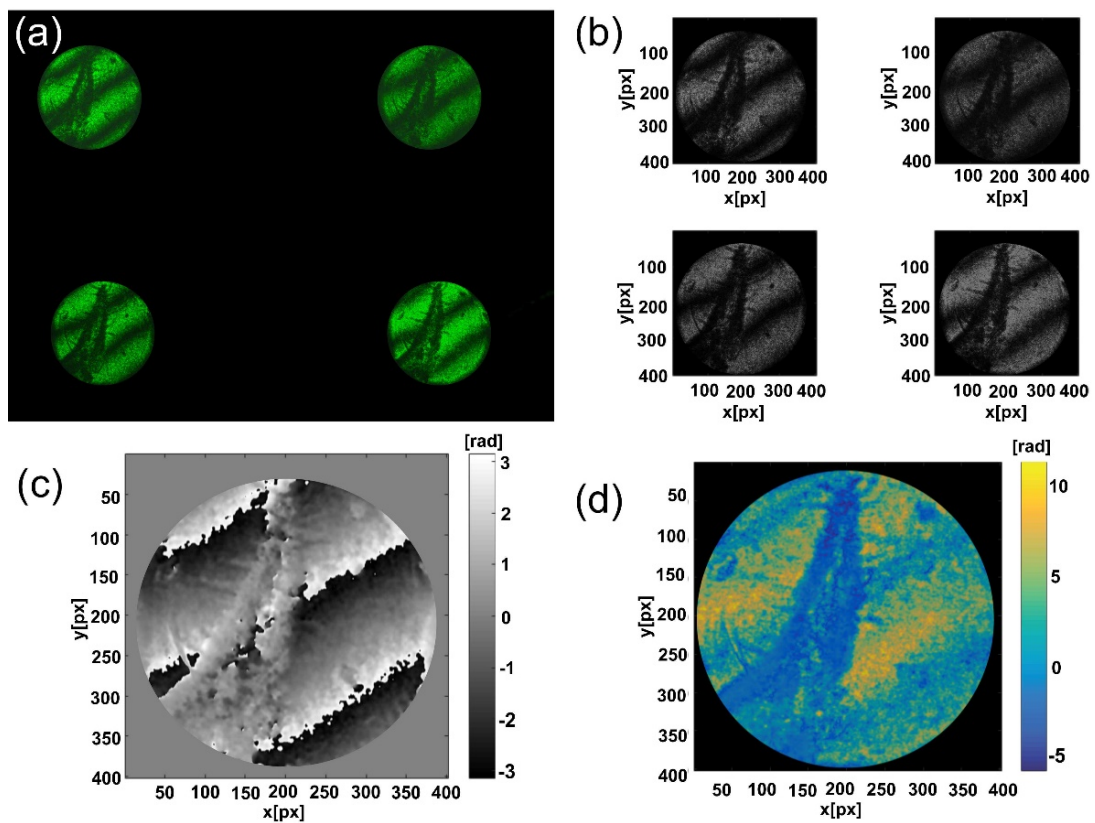
Figure 7. Pseudoscorpion claw. (**a**,**b**) Four simultaneous patterns. (**c**) Wrapped phase. (**d**) Phase map.
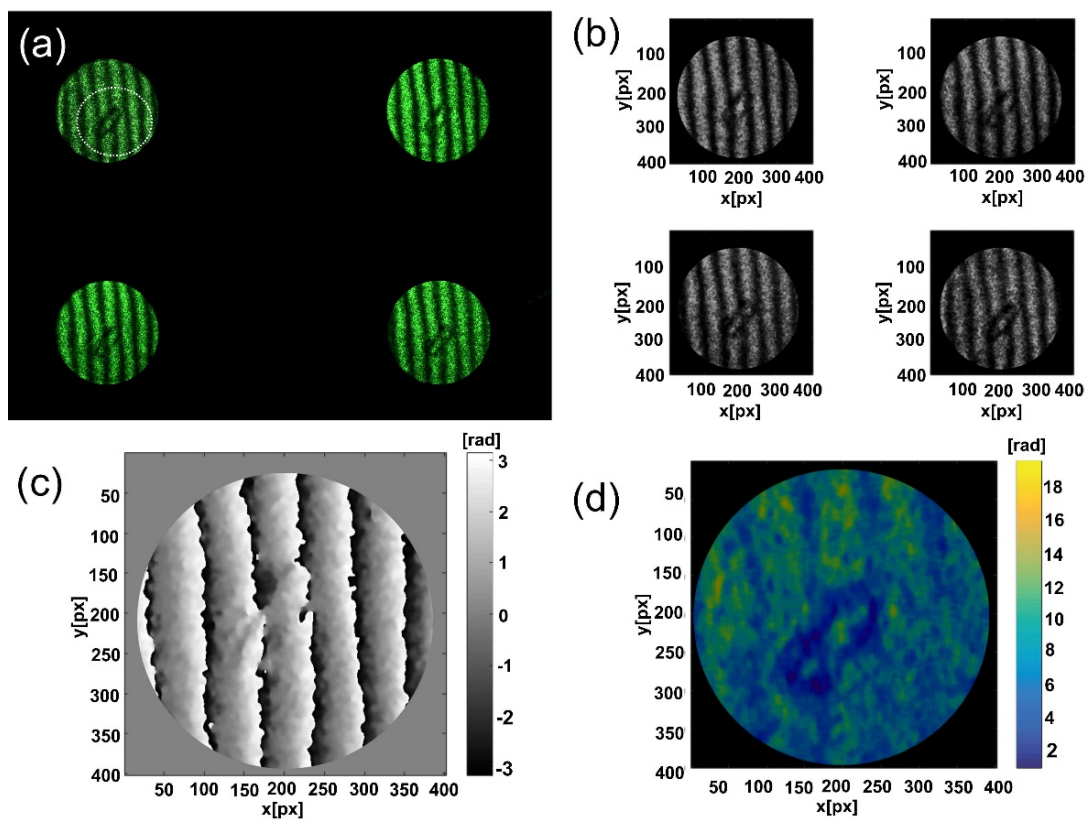

Figure 8. Microarthropod *Collembola*. (**a**,**b**) Four simultaneous patterns. (**c**) Wrapped phase. (**d**) Phase map.
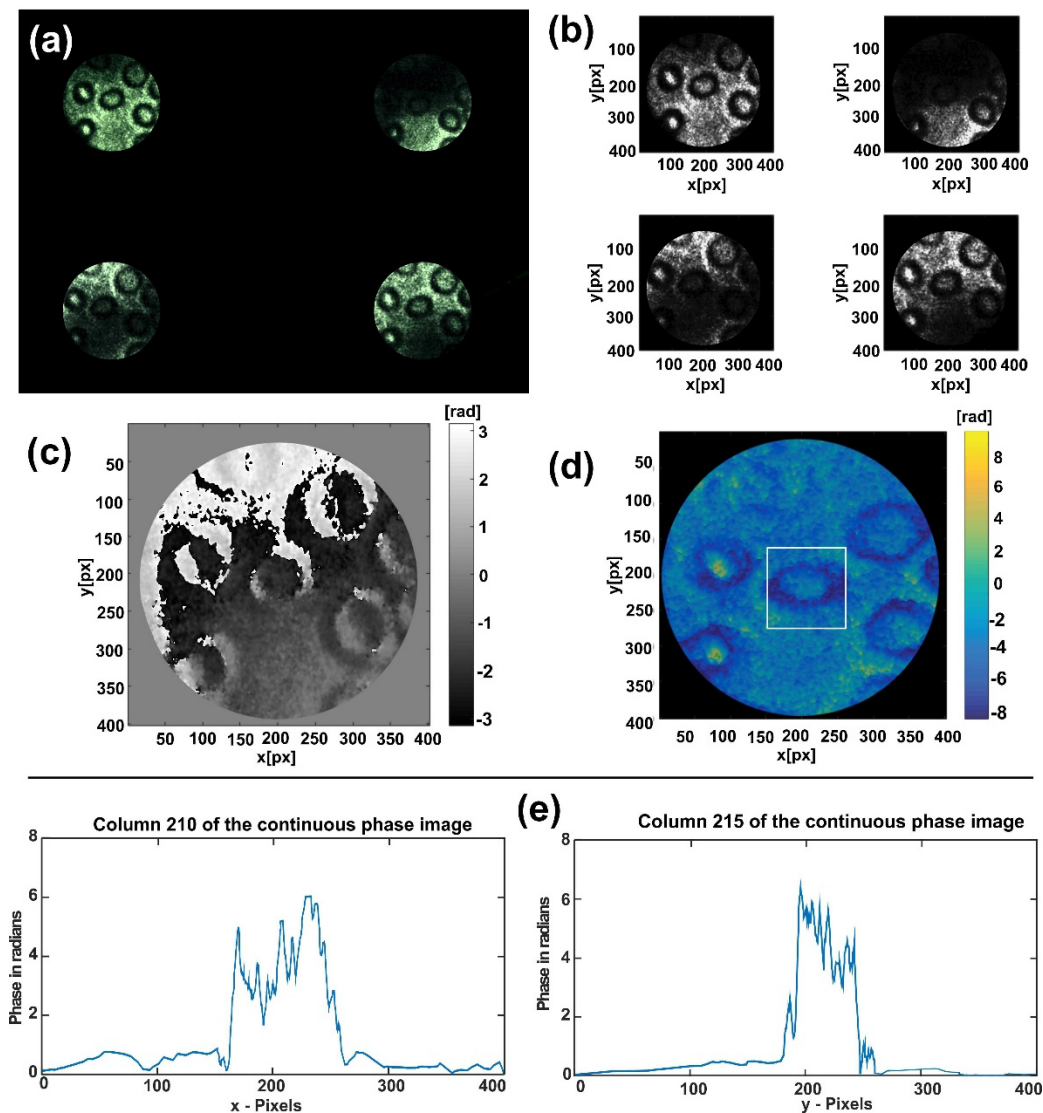
Figure 9. Red blood cells. (**a**,**b**) Four simultaneous patterns. (**c**) Wrapped phase. (**d**) Phase map. (**e**) Transversal section of RBC.

Figure 4 shows a tilted wavefront; Figure 4a shows the four simultaneous patterns used, Figure 4b the preprocessed filtering patterns, and Figure 4c shows the unwrapped phase map. The resulting optical phase map is shown in Figure 4d. Figure 5 shows a wavefront with aberrations generated by placing our collimating lens out of focus and off the optical axis. The obtained patterns, in this case, are displayed in Figure 5a, while the normalized ones can be observed in Figure 5b. Figure 5c shows the wrapped phase, and the optical phase map is shown in Figure 5d.

Figure 6 shows the results obtained by placing an oil layer on a microscope slide; the characteristic patterns of the oil layer are shown in Figure 6a, while Figure 6b presents the preprocessed patterns. Figure 6c shows the unwrapped phase obtained, and Figure 6d presents the optical phase map generated by the oil layer. After stabilizing the oil on the cover slide, the groove of the oil is noticeable on the phase map. Figure 7 shows the results obtained by analyzing a small section of a pseudoscorpion claw. Figure 7a shows the patterns used for processing the optical phase, while Figure 7b presents the preprocessed patterns. Figure 7c shows the wrapped phase, and, in Figure 7d, the calculated phase map is displayed.

Figure 8 presents the experimental results obtained from observing a microarthropod called *Collembola*; Figure 8a shows the four simultaneous patterns used, while Figure 8b the processed patterns. Due to the absorption of the sample, there are regions with high absorption producing errors for the phase calculation; for this reason, a region of interest (ROI) enclosed by a dotted circle (Figure 8a) was selected to process the optical phase. Figure 8c shows the wrapped phase map. The resulting optical phase map is shown in Figure 8d. In Figure 9, the results obtained with human red blood cells (RBCs) fixed on a microscope slide are shown; in this case, a low fringe number was used. Figure 9a,b show the interferograms and the processed patterns, respectively, while, in Figure 9c,d, the wrapped phase and the optical phase maps are presented, respectively. In Figure 9e, the cross-sections along the *xy*-axes of the cell enclosed in a rectangle in Figure 9d are shown; the study of RBC morphology has proven to be very useful in the biomedical sector for diagnosing diseases. In Figure 10, the cases of two and four simultaneous steps are presented for the case of a flat wavefront. The four-step interferograms are shown in Figure 10a, while Figure 10b shows the two-step case with a relative phase of 60°. The phase maps obtained shown in Figure 10c,d present the case of four and two steps, respectively. It can be seen that, for this case, the four-phase step method has errors. This can be seen in Figure 10e, where the cross-section is shown along each method's *x*- and *y*-axes. In Figure 10f a residuals plot is presented, where the average difference between the two methods is 0.42 rad.
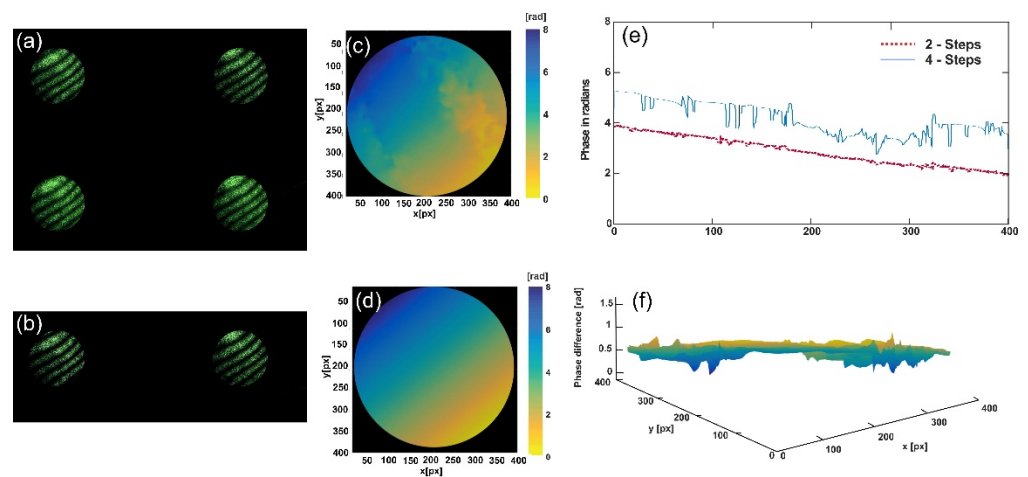

Figure 10. (**a**) Four-interferogram method. (**b**) Two-interferogram method (**c**) Phase map using the four-step algorithm. (**d**) Phase map using the two-step algorithm. (**e**) *xy* cross-section. (**f**) Error.

We analyzed the system's stability by capturing 20 frames at 1 fps to determine the variations at each pixel, as shown in Figure 11. Figure 11a shows the intensity for a representative frame, while, in Figure 11b, we show its corresponding unwrapped phase. Figure 11c shows the temporal mean, and, in Figure 11d, we can see the standard deviation map of the variations per pixel. Our obtained standard deviation resulted in 0.4 rad [34,43,44]; however, systematic errors such as interferogram registration, component conditions, and possible changes in polarization reduce the system response.

One of the advantages of generating simultaneous patterns is the analysis of the temporal variations of a sample. In Figure 12, representative frames of the temporal variation of water flow poured on a microscope slide moving by gravity are shown; the associated video (Supplementary Video S1) shows the temporal evolution of the phase map. The video shows the variations introduced by the phase as it moves. The different levels shown in the results are due to variations in the liquid layer deposited on the slide. For this case, the interferogram was recorded with a resolution of 600 × 600 pixels.

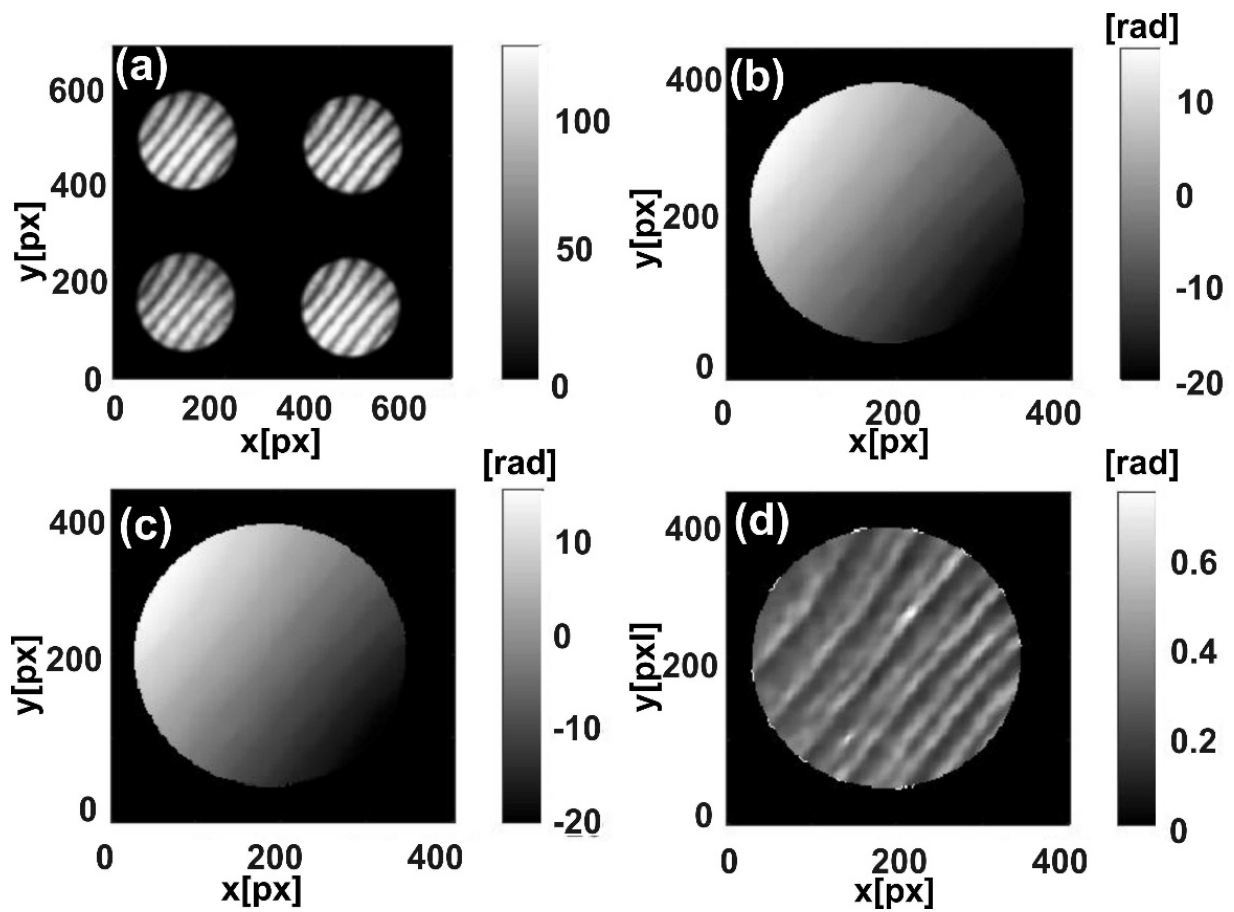**Figure 11.** Stability of the system. (**a**) Intensity: Four phase-shifted interferograms. (**b**) Unwrapped phase for the first frame. (**c**) Mean. (**d**) Standard deviation.
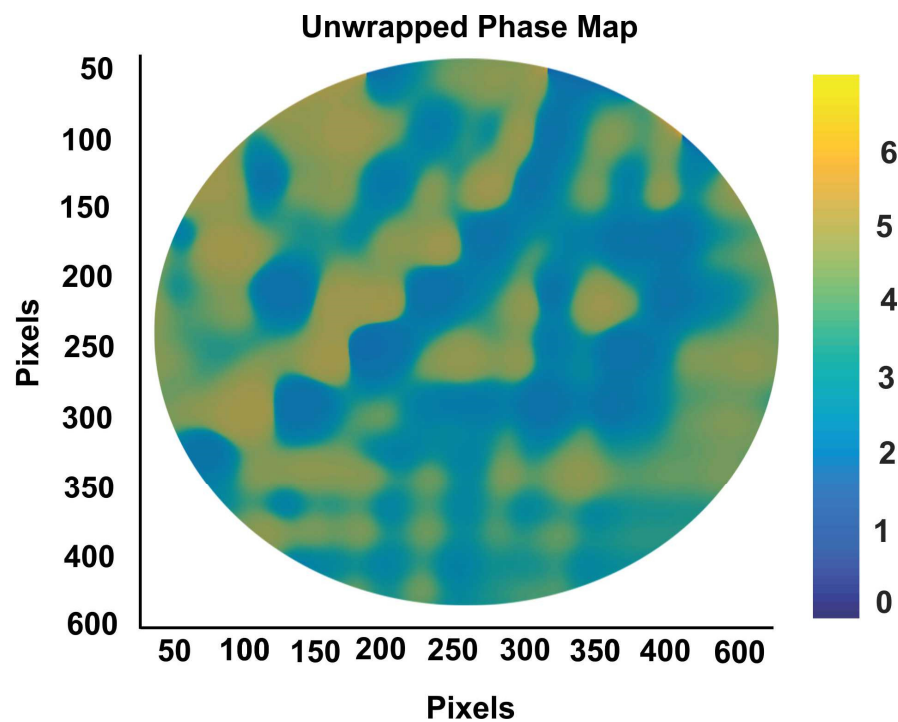

Figure 12. Dynamic phase object. Representative frames (Supplementary Video S1).

6. Discussion

An advantage of using phase shift is capturing multiple images over the same detector field. In general, for high-frequency fringes, the diminishing width of the fringes may exceed the detector array's Nyquist limit, resulting in data dropouts. Since we have low-frequency interferograms with respect to the inverse of pixel spacing (see Figure 5), the influence of errors in the capture seems to be relatively small [45,46]. The implemented system has the limitation of the inherent handling difficulty due to the size of the recovered components, being on the order of 4 mm. In addition, the alignment of such small pieces must be thoroughly carried out, which implies more laboratory time allocation.

However, it should be noted that the elements used are inexpensive and easily accessible; they are handy to test the basic operation process of dynamic interferometers when there is limited or no funding for this kind of research. In general, when using wave retarders and polarizers, phase errors are most evident when the shifts are not $\pi/2$. To verify that the transmitted intensities at the interferometer's output were constant, a polarizer was placed as an analyzer. A full rotation (360°) was performed, measuring intensities every 5° with a potentiometer, verifying that the variations did not exceed 2% of the maximum value measured and, thus, ensuring that the polarization at the output of the PMZI was circular.

Once this was verified, the same procedure was performed on each replicated pattern used in optical phase recovery to verify that the grating did not introduce noticeable changes in the polarization states. To implement the 2×2 polarizing mask, the polarization axis of each linear polarizer involved was marked to be thoroughly fixed in the mask at the appropriate angle. The calibration of the fast angle of such polarizers was made by comparison with a previously calibrated one.

The shape of the calibrated linear polarizers in the mask was modeled and passed to a laser cutting machine. Another limitation found was the quality variation of the recovered components, which changed from one recycled electronic element to another. Such differences can be seen in the results obtained; the phase presented noise and errors due to the quality of the grids and some of the lenses. Another disadvantage of the system was reproducibility. We noticed that the components suffered from environmental changes and deteriorated with the use of the laser; therefore, once an experimental system is set up, all the results needed to validate the experiment must be taken at once. However, these systems can be used to show some applications of basic simultaneous interferometry but, at this stage, cannot be used for specialized and precision research.

7. Conclusions

We presented an interferometric system implemented with recycled optical components to measure the phase maps of phase objects samples. The system uses two crossed recycled gratings to generate replicas of the interferogram. The presented system can be easily implemented for various applications in interferometry in some research areas and in a specialized teaching laboratory. In order to achieve such a level, we must design and build suitable bases and characterize a large number of components to select the best ones.

Author Contributions: N.-I.T.-A., conceptualization, methodology, and software; N.-I.T.-A. and J.M.I.-I., writing—original draft preparation; J.M.I.-I., L.G.-L. and G.R.-L., methodology and software; J.M.I.-I., L.G.-L. and B.C.-P., formal analysis and resources; D.-I.S.-G., A.Q., J.G.O.-M. and B.C.-P., writing—review and editing, and supervision; D.-I.S.-G., A.Q., J.G.O.-M. and J.M.I.-I., data curation and writing—review and editing; N.-I.T.-A., resources and funding acquisition; N.-I.T.-A., conceptualization, investigation, methodology, and supervision. All authors read and agreed to the published version of the manuscript.

References

1. Azapagic, A.; Perdan, S. Indicators of sustainable development for industry: A general framework. *Trans IChemE* **2000**, *78*, 243–261. [CrossRef]
2. Barbier, E.B. The concept of sustainable economic development. *Environ. Conserv.* **1987**, *14*, 101. [CrossRef]
3. Kiddee, P.; Pradhan, J.K.; Mandal, S.; Biswas, J.K.; Sarkar, B. An overview of treatment technologies of E-waste, Chapter 1. In *Handbook of Electronic Waste Management International Best Practices and Case Studies*; Elsevier: Cambridge, MA, USA, 2019; pp. 1–18.
4. Crane, R. Interference Phase Measurement. *Appl. Opt.* **1969**, *8*, 538.
5. Bruning, J.H.; Herriott, D.R.; Gallagher, J.E.; Rosenfeld, D.P.; White, A.D.; Brangaccio, D.J. Digital Wavefront Measuring Interferometer for Testing Optical Surfaces and Lenses. *Appl. Opt.* **1974**, *13*, 2693. [CrossRef] [PubMed]
6. Bruning, J.H. *Fringe Scanning Interferometers, in Optical Shop Testing*; Malacara, D., Ed.; Wiley: New York, NY, USA, 1978.
7. Hardy, J.; Feinleib, J.; Wyant, J.C. Real time phase correction of optical imaging systems, OSA Topical Meeting on Opt. In Proceedings of the Propagation through Turbulence, Boulder, CO, Canada, 9–11 July 1974.
8. Wyant, J.C. Use of an ac Heterodyne Lateral Shear Interferometer with Real-Time Wavefront Correction Systems. *Appl. Opt.* **1975**, *14*, 2622. [CrossRef]
9. Wyant, J.C. Dynamic Interferometry. *Opt. Photonics News* **2003**, *14*, 36–41. [CrossRef]
10. Morris, M.N.; Millerd, J.; Brock, N.; Hayes, J.; Saif, B. Dynamic Phase-Shifting Electronic Speckle Pattern Interferometer. In Proceedings of the Optical Manufacturing and Testing VI, San Diego, CA, USA, 18 August 2005.
11. Serrano-Garcia, D.I.; Toto-Arellano, N.I.; García, A.M.; Álvarez, J.A.R.; Téllez-Quiñones, A.; Rodríguez-Zurita, G. Simultaneous phase-shifting cyclic interferometer for generation of lateral and radial shear. *Rev. Mex. Fis.* **2011**, *57*, 255–258.
12. Serrano-García, D.I.; Toto-Arellano, N.I.; Martínez-García, A.; Zurita, G.R. Radial slope measurement of dynamic transparent samples, J. *Opt.* **2012**, *14*, 045706. [CrossRef]
13. Islas, J.M.I.; Flores-Muñoz, V.H.; Serrano-García, D.-I.; Serrano-Mendoza, J.G.; Sánchez, M.D.; Barraza, A.G. Noel-Ivan Toto-Arellano, Development of a dynamic interferometer using recycled components based on polarization phase shifting techniques. *Opt. Laser Technol.* **2020**, *123*, 105915. [CrossRef]
14. Rodriguez-Zurita, G.; Meneses-Fabian, C.; Toto-Arellano, N.I.; Vázquez-Castillo, J.F.; Robledo-Sánchez, C. One-shot phase-shifting phase-grating interferometry with modulation of polarization: Case of four interferograms. *Opt. Express* **2008**, *16*, 7806–7817. [PubMed]
15. Toto-Arellano, N.I. 4D measurements of biological and synthetic structures using a dynamic interferometer. *J. Mod. Opt.* **2017**, *64* (Suppl. 4), S20–S29. [CrossRef]
16. Shock, I.; Barbul, A.; Girshovitz, P.; Nevo, U.; Korenstein, R.; Shakeda, N.T. Optical phase nanoscopy in red blood cells using low-coherence spectroscopy. *J. Biomed. Opt.* **2012**, *17*, 101509. [CrossRef]
17. Pham, H.; Ding, H.; Sobh, N.; Do, M.; Patel, S.; Popescu, G. Off-axis quantitative phase imaging processing using CUDA: Toward real-time applications. *Biomed. Opt. Express* **2011**, *2*, 1781–1793. [CrossRef] [PubMed]
18. Lee, K.; Kim, K.; Jung, J.; Heo, J.; Cho, S.; Lee, S.; Chang, G.; Jo, Y.; Park, H.; Park, Y. Quantitative Phase Imaging Techniques for the Study of Cell Pathophysiology: From Principles to Applications. *Sensors* **2013**, *13*, 4170–4191. [CrossRef]
19. Marquet, P.; Depeursinge, C.; Magistretti, P.J. Review of quantitative phase-digital holographic microscopy: Promising novel imaging technique to resolve neuronal network activity and identify cellular biomarkers of psychiatric disorders. *Neurophotonics* **2014**, *1*, 020901. [CrossRef]
20. Park, Y.K.; Depeursinge, C.; Popescu, G. Quantitative phase imaging in biomedicine. *Nat. Photonics* **2018**, *12*, 578–589. [CrossRef]
21. Millerd, J.E.; Wyant, J.C. Simultaneous Phase-Shifting Fizeau Interferometer. U.S. Patent 7,057,738 B2, 6 June 2006.
22. Kemper, B.; von Bally, G. Digital holographic microscopy for live cell applications and technical inspection. *Appl. Opt.* **2008**, *47*, A52–A61. [CrossRef] [PubMed]
23. Myung, K.K. Principles and techniques of digital holographic microscopy. *SPIE Rev.* **2010**, *1*, 018005.

24. Malacara, D. *Optical Shop Testing*, 3rd ed.; Wiley: New York, NY, USA, 2007.

25. Hariharan, P. *Basics of Interferometry*; Elsevier Inc.: Cambridge, MA, USA, 2007.

26. Hecht, E. Optics. (Pearson Education, 2016). Available online: https://www.pearson.com/us/higher-education/program/Hecht-Optics-5th-Edition/PGM45350.html (accessed on 1 February 2022).

27. Serrano-García, D.I.; Rayas-Alvarez, J.A.; Arellano, N.I.T.; Rodriguez-Zurita, G.; Pérez, A.M. Adjustable-window grating interferometer based on a Mach-Zehnder configuration for phase profile measurements of transparent samples. *Opt. Eng.* **2012**, *51*, 055601. [CrossRef]

28. Toto-Arellano, N.I.; Flores-Muñoz, V.H.; Lopez-Ortiz, B. Dynamic phase imaging of microscopic measurements using parallel interferograms generated from a cyclic shear interferometer. *Opt. Express* **2014**, *22*, 20185–20192. [CrossRef]

29. Malacara, D.; Servin, M.; Malacara, Z. *Phase Detection Algorithms in interferomgram Analysis for Optical Testing*; Wiley: New York, NY, USA, 2005.

30. Servin, M.; Estrada, J.C.; Quiroga, J.A. The general theory of phase shifting algorithms. *Opt. Express* **2009**, *17*, 21867–21881. [CrossRef] [PubMed]

31. Kerr, D.; Kaufmann, G.H.; Galizzi, G.E. Unwrapping of interferometric phase-fringe maps by the discrete cosine transform. *Appl. Opt.* **1996**, *35*, 810–816. [CrossRef] [PubMed]

32. Ghiglia, D.C.; Romero, L.A. Robust two-dimensional weighted and unweighted phase unwrapping that uses fast transforms and iterative methods. *JOSA A* **1994**, *11*, 107–117. [CrossRef]

33. Vargas, J.; Quiroga, J.A.; Sorzano, C.O.S.; Estrada, J.C.; Carazo, J.M. Two-step interferometry by a regularized optical flow algorithm. *Opt. Lett.* **2011**, *36*, 3485–3487. [CrossRef]

34. Guo, R.; Yao, B.; Gao, P.; Min, J.; Han, J.; Yu, X.; Lei, M.; Yan, S.; Yang, Y.; Dan, D.; et al. Parallel on-axis phase-shifting holographic phase microscopy based on reflective point-diffraction interferometer with long-term stability. *Appl. Opt.* **2013**, *52*, 3484–3489. [CrossRef]

35. Abdelsalam, D.G.; Yao, B.; Gao, P.; Min, J.; Guo, R. Single-shot parallel four-step phase shifting using on-axis Fizeau interferometry. *Appl. Opt.* **2012**, *51*, 4891–4895. [CrossRef] [PubMed]

36. Jung, M.; Jeon, H.; Lim, S.; Hahn, J. Color Digital Holography Based on Generalized Phase-Shifting Algorithm with Monitoring Phase-Shift. *Photonics* **2021**, *8*, 241. [CrossRef]

37. Gao, C.; Gao, Z.; Niu, Y.; Wang, X.; Zhao, J.; Deng, L. An Improved Large-Field Microscopic Speckle Interferometry System for Dynamic Displacement Measurement of MEMS. *Photonics* **2021**, *8*, 271. [CrossRef]

38. Barcelata-Pinzón, A.; Álvarez-Tamayo, R.I.; Prieto-Cortés, P. A Real-Time Automated System for Dual-Aperture Common-Path Interferometer Phase-Shifting. *Appl. Sci.* **2021**, *11*, 7438. [CrossRef]

39. Bello, V.; Simoni, A.; Merlo, S. Spectral Phase Shift Interferometry for Refractive Index Monitoring in Micro-Capillaries. *Sensors* **2020**, *20*, 1043. [CrossRef]

40. Cheng, N.J.; Su, W.H. Phase-Shifting Projected Fringe Profilometry Using Binary-Encoded Patterns. *Photonics* **2021**, *8*, 362. [CrossRef]

41. Quiroga, J.; Servin, M. Isotropic n-dimensional fringe pattern normalization. *Opt. Commun.* **2003**, *224*, 221–227. [CrossRef]

42. Rivera, M.; Dalmau, O.; Gonzalez, A.; Hernandez-Lopez, F. Two-step fringe pattern analysis with a Gabor filter bank. *Opt. Lasers Eng.* **2016**, *85*, 29–37. [CrossRef]

43. Toto-Arellano, N.I.; Serrano-Garcia, D.I.; Rodriguez-Zurita, G. Optical path difference measurements with a two-step parallel phase shifting interferometer based on a modifed Michelson configuration. *Opt. Eng.* **2017**, *56*, 094107. [CrossRef]

44. Min, J.; Yao, B.; Gao, P.; Guo, R.; Zheng, J.; Ye, T. Parallel phase-shifting interferometry based on michelson-like architecture. *Appl. Opt.* **2010**, *49*, 6612–6616. [CrossRef] [PubMed]

45. Duarte, M.F.; Davenport, M.A.; Takhar, D.; Laska, J.N.; Sun, T.; Kelly, K.F.; Baraniuk, R.G. Single-pixel imaging via compressive sampling. *IEEE Signal Processing Mag.* **2008**, *25*, 83–91. [CrossRef]

46. Arvidson, R.S.; Fischer, C.; Sawyer, D.S.; Scott, G.D.; Natelson, D.; Lüttge, A. Lateral Resolution Enhancement of Vertical Scanning Interferometry by Sub-Pixel Sampling. *Microsc. Microanal.* **2014**, *20*, 90–98. [CrossRef]